THE EFFECT OF VELOCITY DISTRIBUTION AND ELECTRON SCREENING ON COLD FUSION

Robert A. Rice, Gary S. Chulick, and Yeong E. Kim

Department of Physics
Purdue University
West Lafayette, Indiana 47907

ABSTRACT

It is demonstrated that electron screening, in combination with a particle velocity distribution, greatly enhances the cross sections and reaction rates for deuteron–deuteron (D–D) and proton–deuteron (p–D) fusion for low kinetic energies ($E \leq 20$ eV, center of mass frame). p–D fusion rates are shown to be comparable to D–D fusion rates for $E \sim 10$ eV, so that in electrolysis experiments with equal amounts of H and D, p–D fusion should compete with D–D fusion as a reaction mechanism.

I. INTRODUCTION

Recently, the effect of a velocity distribution [1] in the context of a surface reaction mechanism [2,3] was shown to be very important in reducing the discrepancy between the electrolysis fusion results [4-9] and the conventional estimates [10-11] of cold fusion rates. More recently, it has been suggested [12] that the effect of electron screening may become significant at low energies and further reduce the discrepancy. In this paper, we present results of our detailed calculations of the deuterium–deuterium (D–D) and proton–deuterium (p–D) fusion rates including both a velocity distribution and electron screening. In section II, definitions and expressions for the Coulomb barrier penetration factor, fusion cross sections and fusion rates are described. In section III, the calculated results are presented and discussed. Finally, section IV contains conclusions.

II. THEORETICAL FORMULATION

Three dominant fusion reactions occurring at low energies are

$$D^+ + D \rightarrow {}^3H(1.01\text{MeV}) + p(3.02\text{MeV}) \,, \quad (1a)$$

$$D^+ + D \rightarrow {}^3\text{He}(0.82\text{MeV}) + n(2.45\text{MeV}) \,, \quad (1b)$$

and

$$\begin{aligned} H^+ \;+\; D &\rightarrow {}^3\text{He} + \gamma(5.5\text{MeV}) \\ \left(\text{or } D^+ \;+\; H \right. &\left. \rightarrow {}^3\text{He} + \gamma(5.5\text{MeV})\right) \end{aligned} \quad (1c)$$

Reaction (1a) is not a "real" fusion reaction but a neutron–transfer reaction, while reaction (1b) is a fusion reaction in which two protons are fused to form a ^{3}He nucleus. Because of the complexity of the four–nucleon system, no rigorous theoretical calculations of the D–D fusion rates and branching ratios and of the H–D fusion rates have been carried out at low positive energies. Since there are no direct measurements of the fusion cross sections, $\sigma(E)$, for reactions (1a) and (1b), below $E_D \lesssim 4$ keV (laboratory (LAB) frame), and for reaction (1c) below $E_H \lesssim 24$ keV (LAB), $\sigma(E)$ has to be extrapolated using the measured values of $\sigma(E)$ at higher energies as is conventionally done in astrophysical calculations [13,14] for $kT \gtrsim 1.5$ keV. In our case, an extrapolation down to the order of 10 eV is required. We describe in the discussion below the extrapolation method used in the astrophysical calculations [13,14] which assumes equal branching ratios for reactions (1a) and (1b). In the following, a theoretical formulation will be given in detail only for reactions (1a) and (1b), as it is similar to that for reaction (1c).

II.1. Velocity Distribution

Since the precise form of the D^+ velocity distribution in electrolysis experiments is not known at present, we will assume a Maxwell–Boltzmann distribution with and without a cut–off for high velocity components. The temperature term, k_BT, will be replaced by the "average" kinetic energy, E_{DD}, in the center of mass (CM) D–D frame, which is related to the most probable velocity v (CM) by $E_{DD} = \frac{M}{2}v^2$ (CM) with the reduced mass $M = M_D/2$.

For a Maxwell–Boltzmann velocity distribution,

the D–D fusion rate, Λ ($\sec^{-1}/D$–D pair), for reaction (1a) or (1b) is given by [13,14]

$$\Lambda(E_{DD}) = \frac{n_D}{2}\,\langle\sigma v\rangle\ , \tag{2}$$

with

$$\langle\sigma v\rangle = \frac{(8/\pi)^{1/2}}{M^{1/2}(E_{DD})^{3/2}}\int_0^{E_c}\sigma(E)E\,e^{-E/E_{DD}}dE\ , \tag{3}$$

where the cross section, $\sigma(E)$, has been parameterized as [13]

$$\sigma(E) = \frac{S(E)}{E}\,e^{-(E_G/E)^{1/2}} \tag{4}$$

which is the conventional form assuming (1a), (1b), and (1c) are non–resonant charged particle reactions. E_G is the "Gamow energy" given by $E_G = (2\pi\alpha Z_D Z_D)^2\ Mc^2/2$ or $E_G \approx 31.39\ (keV)^{1/2}$ with the reduced mass $M \approx M_D/2$ for reactions (1a) and (1b) and $E_G^{1/2} = 25.64\ (\mathrm{keV})^{1/2}$ for reaction (1c) with the reduced mass $M = m_p M_D/(m_p + M_D) \approx M_D/3$. E is in units of keV in the center of mass (CM) reference frame. The S–factor, $S(E)$, is extracted from the experimentally measured values [15,16] of the cross section, $\sigma(E)$, for $E \gtrsim 4$ keV and is nearly constant [13,16], $S(E) \approx 52.9\ \mathrm{keV} - b$, for both reactions (1a) and (1b) in the energy range of interest here, $E \lesssim 1$ keV. For reaction (1c), $S(E) \approx 2.50 \times 10^{-4}\ \mathrm{keV} - b$ [13]. The deuterium density n_D is assumed to be $\sim 6\times10^{22}\ cm^{-3}$. E_C in eq. (3) is the upper integration limit beyond which the high velocity components are cut off. With a Taylor series expansion of $S(E)$ [13]

$$S(E) \approx S(O) + S'(O)E + \frac{1}{2}\,S''(O)E^2\ , \tag{5}$$

the integral in eq. (3) can be carried out numerically.

For a sharp velocity distribution, which has been used in the argument against the possibility of D–D fusion at room temperature, the D–D fusion rate ($\sec^{-1}/D$–D pair), Λ_δ, is given by

$$\Lambda_\delta(E) = \frac{n_D}{2}\,\sigma(E)v(CM) \tag{6}$$

where $E = E_{DD} = \frac{M}{2}\,v^2(CM) = \frac{M_D}{4}\,v^2(LAB) = \frac{1}{2}\,E_D(\mathrm{LAB})$, and $\sigma(E)$ is from eq. (4).

II.2. Electron Screening Effect

In electrolysis fusion experiments and other fusion processes, D^+ is incident on D, which is shielded by electron clouds and is electrically neutral outside the electron screening range, r_s. The expression for $\sigma(E)$ given by eq. (4) is derived for the case in which one D^+ is incident on another D^+. Therefore, the Coulomb barrier penetration factor ("Gamow factor") in eq. (4)

$$P_G(E) = \exp\left(-(E_G/E)^{1/2}\right) \tag{7}$$

is appropriate only for the $(D^+ + D^+)$ reaction and needs to be modified for the case of $(D^+ + D)$ in reactions (1a) and (1b), and for the case of $(D^+ + H)$ in reaction (1c). The modified Coulomb barrier penetration factor, $P_s(E)$, is the probability of tunneling through the barrier to reach the nuclear surface and can be computed from solutions of the Schroedinger equation for a $(D^+ + D)$ system in which an attractive Coulomb potential $V_s(r)$ due to the presence of shielding electrons is included with the original repulsive Coulomb potential between two D^+'s (two protons).

The modified Coulomb barrier penetration factor, $P_s(E)$, which includes the effect of $V_s(r)$, can be calculated in the Wentzel–Kramers–Brillouin (WKB) approximation as

$$P_s(E) = \exp\left[-2\left(\frac{2M}{\hbar^2}\right)^{1/2}\int_{r_N}^{r_a}(V_c(r) + V_s(r) - E)^{1/2}dr\right] \tag{8}$$

where $V_c(r)$ is the repulsive Coulomb potential between two D^+'s,

$$V_c(r) = \frac{Z_D Z_D e^2}{r}\ , \tag{9}$$

and $V_s(r)$ is the potential due to the shielding electrons. The effective nuclear interaction range, $r_N \approx 8F$ (twice the deuteron radius), can be set to zero in eq. (8) without loss of accuracy. The integral in eq. (8) cannot be carried out analytically in general, but can be written for an attractive potential, $V_s(r) < 0$, as

$$2\left(\frac{2M}{\hbar^2}\right)^{1/2}\int_0^{r_a}(V_c(r) + V_s(r) - E)^{1/2}dr = \frac{(E_G)^{1/2}}{(E + E_s(E))^{1/2}} \tag{10}$$

where $E_s(E)$ is determined by carrying out the integral numerically for each value of $E > 0$. The modified penetration factor, $P_s(E)$, is then given by

$$P_s(E) = \exp\left(-E_G^{1/2}/(E + E_s(E))^{1/2}\right) . \quad (11)$$

When $V_s(r) = 0$, $E_s(E)$ vanishes, and we recover the conventional Gamow factor, $P_s(E) = P_G(E)$, given by eq. (7).

The classical turning point, r_a in eq. (8), is determined by

$$V_c(r_a) + V_s(r_a) = E . \quad (12)$$

From eqs. (10) and (12), it can be easily shown that $E_s(E)$ in eqs. (10) and (11) satisfies $|V_s(r_a)| < E_s(E) < |V_s(0)|$ [12]. Using $P_s(E)$, the new extrapolation formula appropriate for reactions (1a), (1b), (1c), and other fusion reactions can now be written as

$$\sigma_s(E) = \frac{S(E)}{E} \exp\left(-E_G^{1/2}/(E + E_s(E))^{1/2}\right) . \quad (13)$$

The parameterization [13] of $S(E)$ used in eq. (4) can also be used in eq. (13), since $S(E)$ is determined from the measured cross sections at higher energies $E \gg E_s(E)$ where the electron screening effect is negligible.

The screening energy term $E_s(E)$ can be extracted from the measured values [15,16] of $\sigma_{\rm exp}(E)$ for reaction (1a), $D(D,p)^3$H. The values of $E_s(E)$ extracted from $\sigma_{\rm exp}(E < 4$ keV$(CM))$ [15,16] using eq. (13) are $(40 - 60)$ eV [12] and have large uncertainties. Therefore, it is important to carry out precise measurements of $\sigma_{\rm exp}(E)$ with improved accuracies for $E < 4$ keV(CM). The experimental values $\sigma_{\rm exp}(E)$ [15,16] were measured with D_2 gas targets for which the electron screening potential is expected to be approximately that of the $1s$ hydrogen electron with $E_s(E) = e^2/a_0 \approx 27$ eV. However, for solid targets such as TiD and PdD, the electron screening range could be as small as a tenth of the Bohr radius, $a_0/10 \approx 0.05$ Å [17]. Thus the extracted values of $E_s(E)$ from solid metal deuteride targets may be up to ten times ($E_s(E) \approx 300$ eV) larger than values ($E_s(E) \approx 40 - 60$ eV) extracted from D_2 gas targets [15,16].

For the case of the Yukawa screening potential, $V(r) = (Z_D Z_s e^2/r)e^{-r/r_s}$, the electron screening potential is given as

$$V_s(r) = V(r) - V_c(r) = -\frac{Z_D Z_s e^2}{r}\left(1 - e^{-r/r_s}\right) . \quad (14)$$

Since the magnitude of $V_s(r)$ decreases monotonically from a maximum value of $|V_s(0)|$ to $|V_s(r_a)|$ as r increases from 0 to r_a, $E_s(E)$ is bounded by

$$\frac{Z_D Z_s e^2}{r_a}\left(1 - e^{-r_a/r_s}\right) < E_s(E) < \frac{Z_D Z_s e^2}{r_s} . \quad (15)$$

The recent elaborate calculations [17,18] yield $r_s \gtrsim 0.05$ Å. $r_s \approx 0.05$ Å for TiD and PdD can be justified also on physical grounds since the electron number density in the solid phase is expected to be 10^3 times larger than that in the gas phase; hence a radius scale such as r_s is expected to be 10 times smaller.

Since the precise form of the effective electron screening potential, $V_s(r)$, will depend on experimental conditions and is not yet known, we shall use a simple potential of the form

$$V_s(r) = -\frac{Z_D Z_s}{r_s}\Theta(r_a - r) \quad (16)$$

which has one parameter Z_s/r_s, where Z_s is the effective electron charge and r_s is the screening radius. $V_s(r)$ given by eq.(16) can be generated from a spherical shell charge distribution, $\rho_e = (Z_s e/4\pi r_s r_a)\delta(r - r_a)$. When $V_s(r)$ given by eq. (16) is used in eq. (8), the penetration factor becomes

$$\tilde{P}_s(e) = \exp\left(-E_G^{1/2}/(E + \tilde{E}_s)^{1/2}\right) \quad (17)$$

where $\tilde{E}_s = Z_D Z_S e^2/r_s = E_s(E)$. Equation (17) has previously been used for D_2 molecular fusion calculations [11] and for the analysis of D_2O cluster fusion [19]. Finally, for the screening potential of eq. (16), eq. (13) becomes

$$\sigma_s(E) = \frac{S(E)}{E} \exp\left(-E_G^{1/2}/\left(E + \tilde{E}_s\right)^{1/2}\right) . \quad (18)$$

III. RESULTS

We calculate the fusion cross sections and reaction rates, σ_{DD} (E_{DD}) and $\Lambda_{DD}(E_{DD})$, using eqs. (18) and (2), respectively, for reactions (1a) and (1b) for $\tilde{E}_s = 0, 1, 4$, and 10 e^2/a_0. n_D is assumed to be 6×10^{22} cm^{-3} and the parametric values for $S(E)$

given in reference 13 are used in eq. (18). The calculated results for $\sigma_{DD}(E_{DD})$ and $\Lambda_{DD}(E_{DD})$ are plotted as functions of $E_{DD} \leq 20$ eV in Figs. 1 and 2, respectively; $\Lambda_{DD}(E_{DD})$ is for the sum of reactions (1a) and (1b), assuming equal branching ratios. In evaluating $\Lambda_{DD}(E_{DD})$, the cut–off energy E_c in eq. (3) is assumed to be infinite. The case where $\tilde{E}_s = 0$ in Figs. 1 and 2 corresponds to the use of the conventional Gamow factor, eq. (7), as in eq. (4). As can be seen from Figs. 1 and 2, the electron screening effect ($\tilde{E}_s \neq 0$) becomes increasingly significant for $\sigma_{DD}(E_{DD})$ and $\Lambda_{DD}(E_{DD})$ for reactions (1a) and (1b), as E_{DD} decreases below 20 eV.

In order to study the effect of the velocity distribution, we calculate the fusion rates $\Lambda_\delta(E_{DD})$ with a sharp (delta function) velocity distribution using eq. (6) for reactions (1a) and (1b). The calculated results for $\Lambda_\delta(E_{DD})$ with $\tilde{E}_s = 0$, 4, and 10 e^2/a_0 are plotted and compared in Fig. 3 with the corresponding cases of $\Lambda_{DD}(E_{DD})$ with a Maxwell–Boltzmann velocity distribution. As can be seen from comparing Λ_δ and Λ_{DD} in Fig. 3, the effect of the velocity distribution becomes increasingly important as E_{DD} decreases, but is less so as $\tilde{E}_s$ increases for reactions (1a) and (1b).

To study the effect of introducing a high–energy cut–off (E_c in eq. (3)) for the Maxwell–Boltzmann velocity distribution, we calculate the fusion rates $\Lambda_{DD}(E_{DD})$ of eq. (2) for the sum of reactions (1a) and (1b) as a function of E_c for the cases $E_{DD} = 5$ and 10 eV with $\tilde{E}_s = 0$, 4, and 10 e^2/a_0 in eq. (18). The calculated results are plotted in Fig. 4. As can be seen from Fig. 4, the effect of a cut–off in the velocity distribution is substantially less for the case of $\tilde{E}_s = 10$ e^2/a_0 than for the case of $\tilde{E}_s = 0$ (no electron screening effect).

For reaction (1c), we calculate the fusion cross section and rates, $\sigma_{pD}(E_{pD})$ and $\Lambda_{pD}(E_{pD})$, using eqs. (18) and (2), respectively, with the replacements of $n_D/2$ in eq. (2) and M and E_{DD} in eq. (3) by n_H, $M = m_p M_D/(m_p + M_D) \approx M_D/3$, and $E_{pD}(CM)$, respectively. Parametric values of $\tilde{E}_s = 0$, 1, 4, and 10 e^2/a_0 are used. n_H is assumed to be $n_H = n_D = 6 \times 10^{22}$ cm^{-3}, and the parametric values for $S(E)$ for reaction (1c) given in reference 13 are used in eq. (18). E_c in eq. (3) is set to infinity. The calculated results for $\sigma_{pD}(E_{pD})$ and $\Lambda_{pD}(E_{pD})$ are plotted in Figs. 5 and 6, respectively. The $\tilde{E}_s = 0$ case in Figs. 5 and 6 corresponds to the use of the conventional Gamow factor,

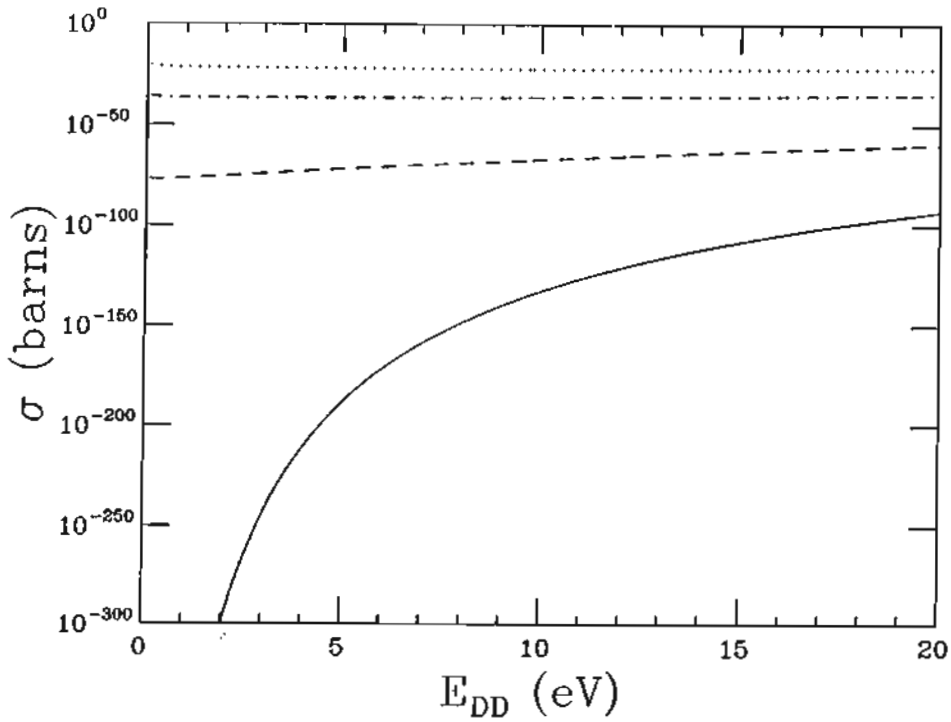

Fig. 1. The calculated cross sections $\sigma_{DD}(E_{DD})$ for reactions (1a) and (1b), $D(D,p)^3H$ and $D(D,n)^3$He, for $E_{DD} \leq 20$ eV with $\tilde{E}_s = 0$, 1, 4, and 10 e^2/a_0. $e^2/a_0 = 27.17$ eV with $a_0 = 0.53$ Å. In this and subsequent figures, the solid, dashed, dash–dotted, and dotted lines refer to the results of calculations using $\tilde{E}_s = 0$, 1, 4, and 10 e^2/a_0, respectively.

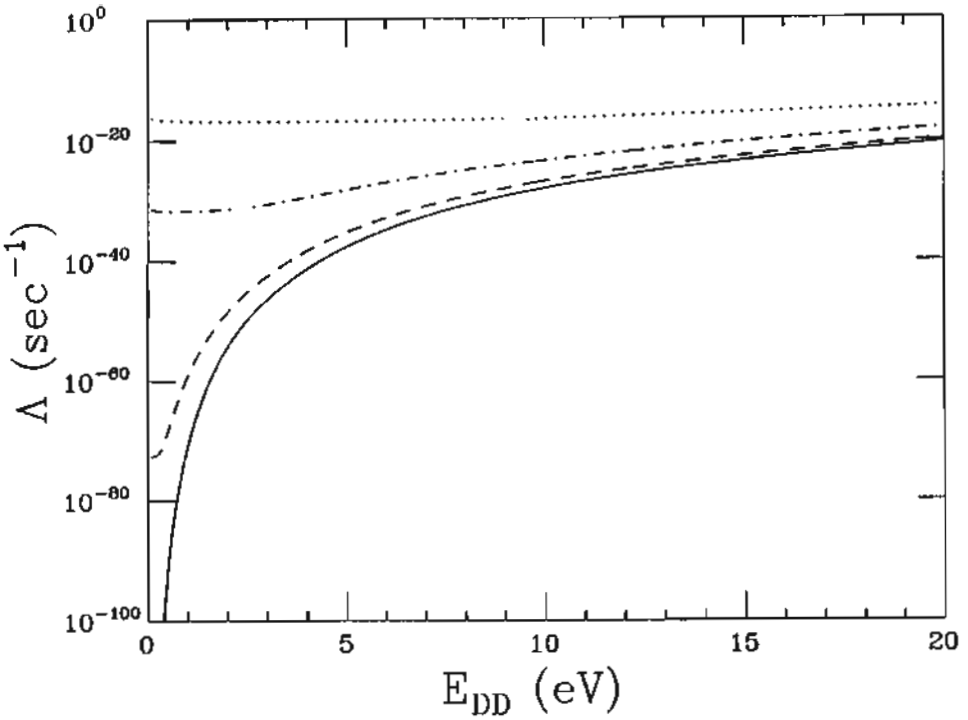

Fig. 2. The calculated fusion rates $\Lambda_{DD}(E_{DD})$ for reactions (1a) and (1b), $D(D,p)^3H$ and $D(D,n)^3$He, for $E_{DD} \leq 20$ eV with $\tilde{E}_s = 0$, 1, 4, and 10 e^2/a_0.

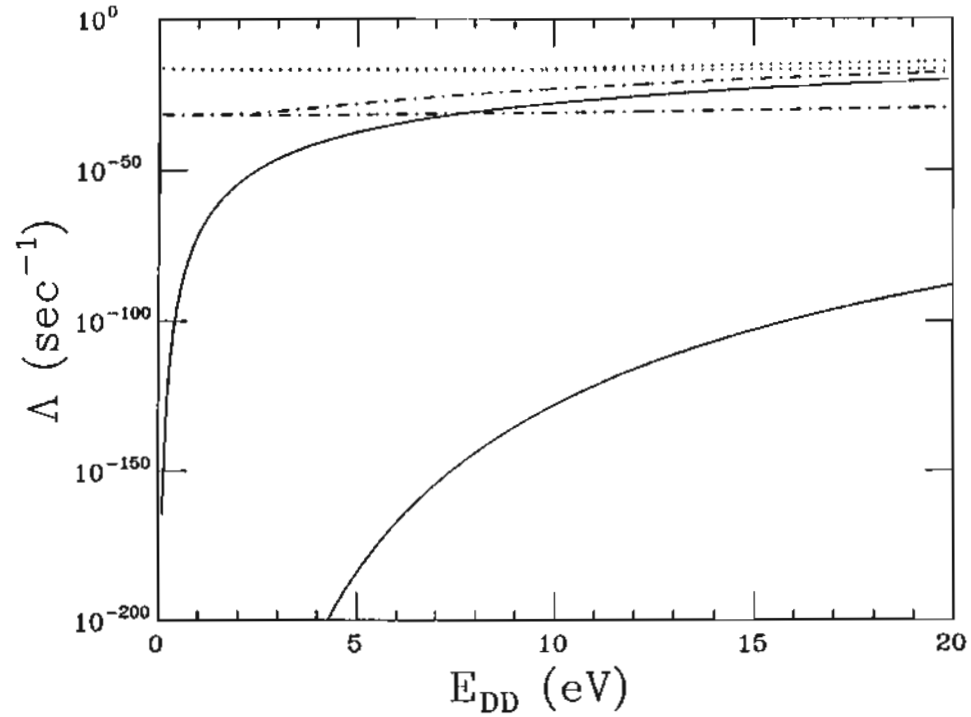

Fig. 3. Comparison of the D–D fusion rates $\Lambda_{DD}(E_{DD})$ with a Maxwell–Boltzmann velocity distribution (upper curve in each pair) and the D–D fusion rates $\Lambda_\delta(E_{DD})$ with a sharp velocity distribution (lower curve in each pair) with $\tilde{E}_s = 0$, 4, and 10 e^2/a_0. $E_{DD} < 20$ eV.

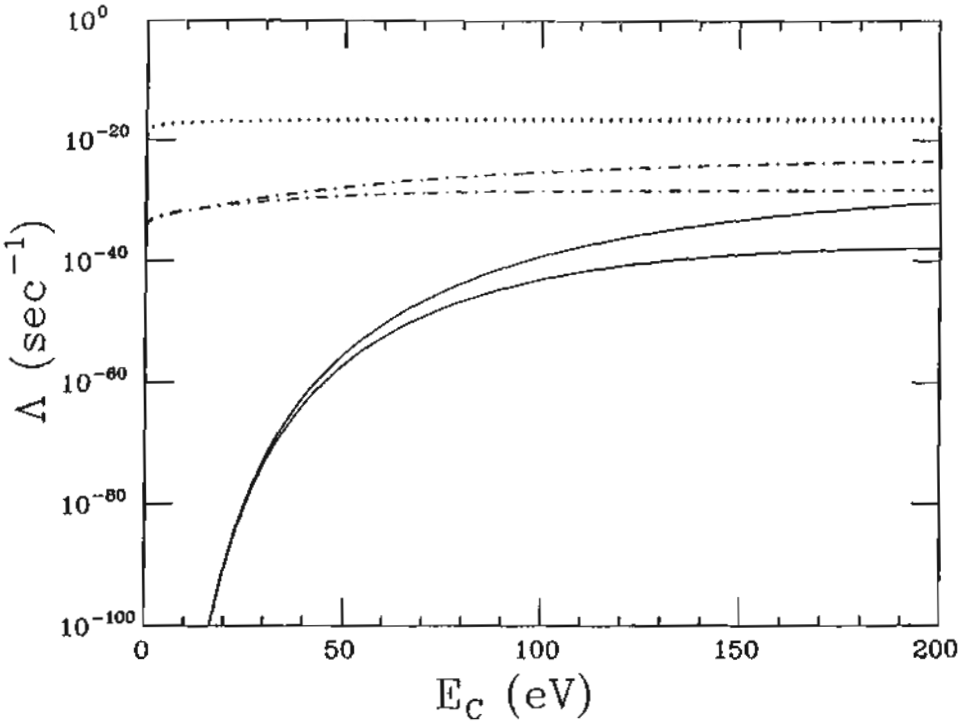

Fig. 4. The calculated D–D fusion rates $\Lambda_{DD}(E_{DD})$ as a function of the cut–off energy E_c with a Maxwell–Boltzmann velocity which is cut off above $E = E_c$. $E_{DD} = 5$ (lower curve in each pair) and 10 eV (upper curve in each pair) with $\tilde{E}_s = 0$, 4, and 10 e^2/a_0 are shown.

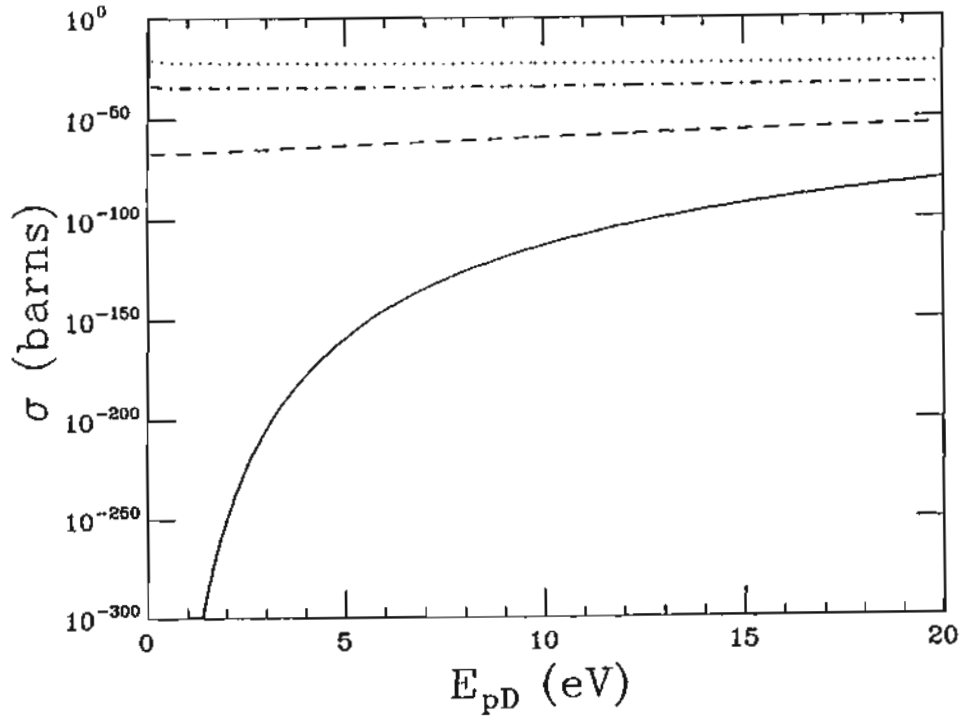

Fig. 5. The calculated cross sections $\sigma_{pD}(E_{pD})$ for reaction (1c), $D(p,\gamma)^3$He, for $E_{pD} \leq 20$ eV with $\tilde{E}_s = 0$, 1, 4, and 10 e^2/a_0.

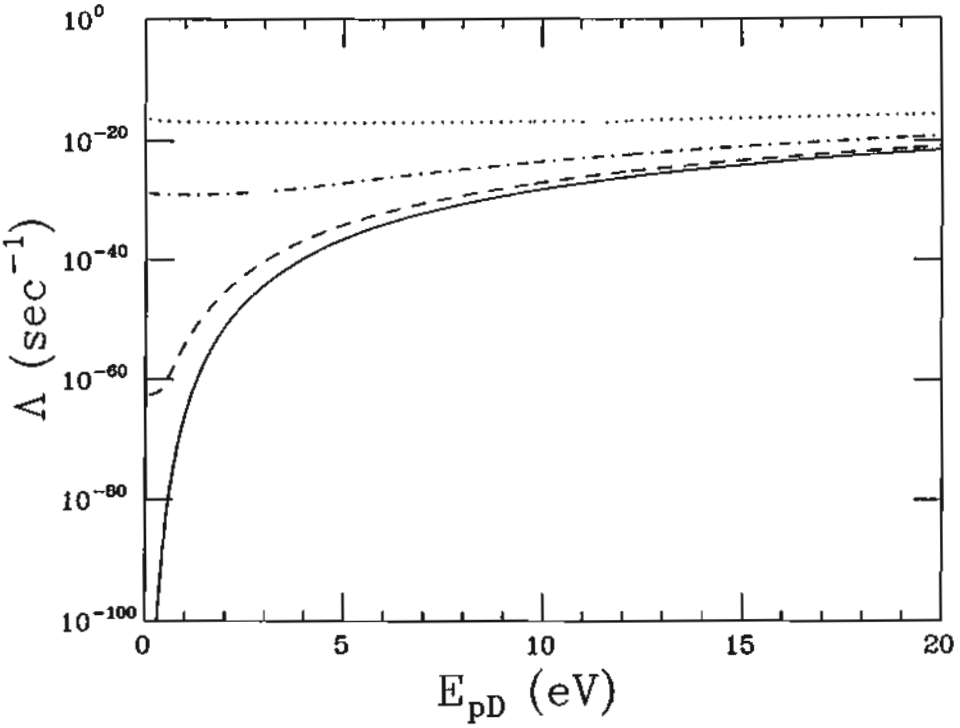

Fig. 6. The calculated fusion rates $\Lambda_{pD}(E_{pD})$ for reaction (1c), $D(p,\gamma)^3$He, for $E_{pD} < 20$ eV with $\tilde{E}_s = 0$, 1, 4, and 10 e^2/a_0.

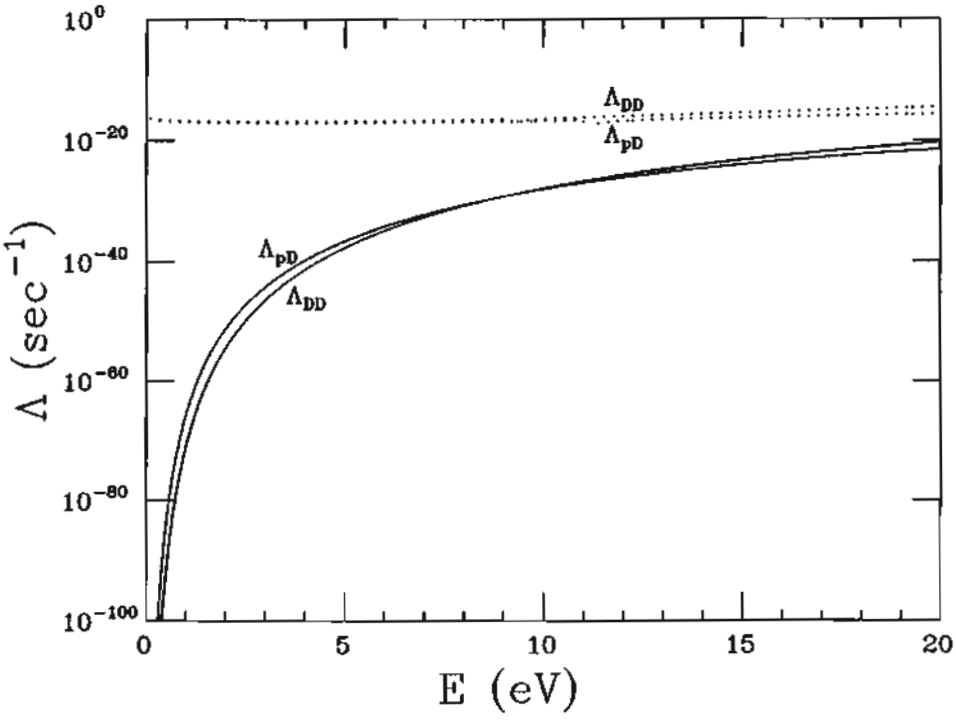

Fig. 7. Comparison of the p–D fusion rates $\Lambda_{pD}(E_{pD})$ and the D–D fusion rates $\Lambda_{DD}(E_{DD})$ for $E(= E_{pD} = E_{DD}) \leq 20$ eV with $\tilde{E}_s = 0$ and 10 e^2/a_0.

eq. (7), as in eq. (4). As in the case of reactions (1a) and (1b) (Figs. 1 and 2), the electron screening effect ($\tilde{E}_s \neq 0$) becomes substantial for $\sigma_{pD}(E_{pD})$ and $\Lambda_{pD}(E_{pD})$ at very low energies.

In order to see whether reaction (1c) will compete with reactions (1a) and (1b) in electrolysis experiments, we compare $\Lambda_{pD}(E_{pD})$ and $\Lambda_{DD}(E_{DD})$ in Fig. 7 for the cases $\tilde{E}_s = 0$ and $10\ e^2/a_0$. As can be seen from Fig. 7, $\Lambda_{pD}(E_{pD})$ is comparable to $\Lambda_{DD}(E_{DD})$ for the case ($\tilde{E}_s \neq 0$) and $n_H = n_D$. Therefore, for a typical value of the H/D ratio, $n_H/n_D \approx 10^{-3}$, in electrolysis experiments, reactions (1a) and (1b) will dominate over reaction (1c). However, reaction (1c) can compete with reactions (1a) and (1b) if $n_H \approx n_D$ is maintained in electrolysis experiments.

IV. CONCLUSIONS

It is shown that the effect of electron screening in conjunction with a particle velocity distribution greatly enhances the cross sections and reaction rates for D–D and p–D fusion at kinetic energies $E \lesssim 20$ eV (CM).

The D–D fusion rate for reaction (1a), $\Lambda^T_{exp}(1a) \approx 10^{-19}\ sec^{-1}$, inferred by Fleischmann et al. [4] from the measurement of tritium production, and also the D–D fusion rate for reaction (1b), $\Lambda^n_{exp}(1a) \approx 10^{-23}\ sec^{-1}$, obtained by Jones et al. [5] are often criticized as being impossible or incorrect when compared to estimates of Λ in bulk matter (an upper limit of $\Lambda \lesssim 10^{-47}\ sec^{-1}$) [10] or to the result of Λ_δ shown in Fig. 3 (lowest curve). Our results for Λ (upper curves) shown in Fig. 3 indicate $\Lambda^n_{exp}(1b) \approx 10^{-23}\ sec^{-1}$ [5] and $\Lambda^T_{exp}(1b) \approx 10^{-19}\ sec^{-1}$ [4] are consistent with calculated values of $\Lambda_{DD}(E_{DD}) \approx 10^{-23}\ sec^{-1}$ and $\Lambda_{DD}(E_{DD}) \approx 10^{-19}\ sec^{-1}$ for $E_{DD} \approx 10$ eV and 17 eV, respectively, with $\tilde{E}_s = 4e^2/a_0$. Therefore, the claimed values of $\Lambda^n_{exp}(1b)$ and $\Lambda^T_{exp}(1a)$ are physically acceptable values for the D–D fusion rate in electrolysis experiments if the applied potentials are 20 V and 34 V, respectively.

To match the D–D fusion rate $\Lambda_{DD}(E_{DD})$ from eq. (1a) to the rate, $\Lambda^{heat}_{exp}(1a) \approx 10^{-10}\ sec^{-1}$ [4] inferred from excess heat measurements [3,5,6], an "average" kinetic energy of $E_{DD} \approx 70$ eV is needed with $\tilde{E}_s = 4\ e^2/a_0$, or $E_{DD} < 70$ eV for $\tilde{E}_s > 4\ e^2/a_0$.

The calculated p–D fusion rates $\Lambda_{pD}(E_{pD})$ for reaction (1c) are comparable to the D–D fusion rates for reactions (1a) and (1c) with $\tilde{E}_s = 10\ e^2/a_0$ and E_{pD}(and E_{DD}) < 20 eV as shown in Fig. 7. Therefore, p–D fusion can compete with D–D fusion if an H/D ratio of $n_H/n_D \approx 1$ can be maintained in both the H_2O–D_2O mixture and the Pd cathode during electrolysis fusion experiments.

REFERENCES

1. R.A. Rice, G.S. Chulick, Y.E. Kim, and J.-H. Yoon, "The Role of Velocity Distribution in Cold Deuterium-Deuterium Fusion," Purdue Nuclear Theory Group Report PNTG-90-5 (January 1990), to be published in Fusion Technology.

2. Y.E. Kim, "Nuclear Theory Hypotheses for Cold Fusion," to be published in the Proceedings of the NSF/EPRI Workshop on Anomalous Effects in Deuterated Metals, Washington, D.C., October 16-18, 1989.

3. Y.E. Kim, "Fission-induced inertial confinement hot fusion and cold fusion with electrolysis," to be published in LASER INTERACTION AND RELATED PLASMA PHENOMENA, Volume 9 (H. Hora and G.H. Miley eds.).

4. M. Fleischmann and S. Pons, "Electrochemically Induced Nuclear Fusion", J. of Electroanal. Chem. **261**, 301 (1989); and errata **263**, 187 (1989).

5. S.E. Jones et al., "Observation of Cold Nuclear Fusion in Condensed Matter," Nature **338**, 737 (27 April 1989).

6. A.J. Appleby, S. Srinivasan, Y.J. Kim, O.J. Murphy, and C.R. Martin, "Evidence for Excess Heat Generation Rates During Electrolysis of D_2O in LiOD using a Palladium Cathode—a Microcalorimetric Study," in the Proceedings of the Workshop on Cold Fusion Phenomena, May 23-25, 1989, Santa Fe, New Mexico, to be published in J. Fusion Energy, March 1990.

7. A. Belzner, U. Bischler, G. Crouch-Baker, T.M. Gur, G. Lucier, M. Schreiber, and R. Huggins "Two Fast Mixed-conductor Systems: Deuterium and Hydrogen in Palladium-Thermal Measurements and Experimental Considerations," in the Proceedings of the Workshop on Cold Fusion Phenomena, May 23-25, 1989, Santa Fe, New Mexico, to be published in J. Fusion Energy, March 1990.

8. K.L. Wolf, N.J.C. Packham, D.R. Lawson, J. Shoemaker, F. Cheng, and J.C. Wass, "Neutron Emission and the Tritium Content Associated with Deuterium Loaded Palladium and

Titanium Metals," in the Proceedings of the Workshop on Cold Fusion Phenomena, May 23-25, 1989, Santa Fe, New Mexico, to be published in J. Fusion Energy, March 1990.

9. P.K. Iyengar, "Cold Fusion Results in BARC Experiment," in the Proceedings of the 5th International Conference on Emerging Nuclear Energy Systems (ICENES V), Karlsruhe, West Germany, July 3-6, 1989.

10. A.J. Leggett and G. Baym, "Exact Upper Bound on Barrier Penetration Probabilities in Many-Body Systems: Application to Cold Fusion," Phys. Rev. Lett. **63**, 191 (1989).

11. K. Langanke, H.J. Assenbaum, and C. Rolfs, "Screening Corrections in Cold Deuterium Fusion Rates," Z. Phys. A. Atomic Nuclei **333**, 317 (1989).

12. Y.E. Kim, "Surface Reaction Mechanism and Lepton Screening for Cold Fusion with Electrolysis," to be published in the Proceedings of the First Annual Conference on Cold Fusion, Salt Lake City, Utah, March 28-31, 1990.

13. W.A. Fowler, G.R. Caughlan, and B.A. Zimmermann, "Thermonuclear Reaction Rates," Ann. Rev. Astr. Astrophys. **5**, 525 (1967); "Thermonuclear Reaction Rates II," **13**, 69 (1975).

14. M.J. Harris, W.A. Fowler, G.R. Caughlan, and B.A. Zimmerman, "Thermonuclear Reaction Rates III," Ann. Rev. Astr. Astrophys. **21**, 165 (1983).

15. A. von Engel and C.C. Goodyear, "Fusion Cross-Section Measurements with Deuterons of Low Energies," Proc. Roy. Soc. A **264**, 445 (1961).

16. A. Krauss, H.W. Becker, H.P. Trautvetter, and C. Rolfs, "Low-Energy Fusion Cross Sections of D+D and D + ^{3}He Reactions," Nucl. Phys. **A465**, 150 (1987).

17. S.N. Vaidya and Y.S. Mayya, "Theory of Screening–Enhanced D–D Fusion in Metals," Jap. J. Appl. Phys. **28**, L2258 (1989).

18. K.B. Whaley, "Boson Enhancement of Finite–Temperature Coherent Dynamics for Deuterium in Metals," Phys. Rev. **B41**, 3473 (1990).

19. M. Rabinowitz and D.H. Worledge, "An Analysis of Cold and Lukewarm Fusion," to be published in Fusion Technology **17**, (1990).